Licence / Master Science de la matière
École Normale Supérieure de Lyon
Université Claude Bernard Lyon I

Internship 2015–2016
Clément Duval
L3 Physique

Simulation of Smith-Purcell radiation following a van den Berg approach

Abstract
New generations of particle accelerators need accurate beam diagnostics. In order to measure the longitudinal profile of electron bunches, a promising non-invasive technique has been developed, using coherent Smith-Purcell radiation. Smith-Purcell radiation is emitted when a relativistic electron passes over a periodic structure. This report presents a method to simulate this radiation according to the van den Berg model, which describes the incident electron as a set of evanescent plane waves. The work is restricted to emitted radiations that belong to the plane of incidence, but there could be a theoretical extension to a more general description based on *conical* diffraction.

Keywords
Diffraction gratings, RCWA, Smith-Purcell radiation, van den Berg model

Internship supervised by:
Nicolas Delerue
delerue@lal.in2p3.fr
Laboratoire de l'Accélérateur Linéaire (LAL)
Centre scientifique d'Orsay,
Bâtiment 200,
91440 Orsay.
https://groups.lal.in2p3.fr/etalon/

Laboratoire de l'Accélérateur Linaire
Université Paris-Sud

22nd July 2016

Contents

Introduction

Background In 1953, Smith and Purcell discovered a radiation emitted by a relativistic charge upon a metallic diffraction grating [1]. They discovered that the wavelength of this radiation is given by

$$\lambda = \frac{d}{n}\left(\frac{1}{\beta} - \cos\theta\right)$$

where n is an integer known as the *order*, $\beta = \frac{v_0}{c}$ is the relativistic parameter. θ and d are defined on Fig. 1. Several ideas have been developed to explain it since then. Two theories have been particularly developed: the so called "induced currents model" and the "van den Berg's model".
The first one uses the classical electrodynamic description of induced currents due to a passing charge close to a perfectly conducting material: because of the non-plane surface, the current is accelerated and thus radiates an electromagnetic field in the upper half-plane [2]. Each groove acts as an independent source and interferes with the others.

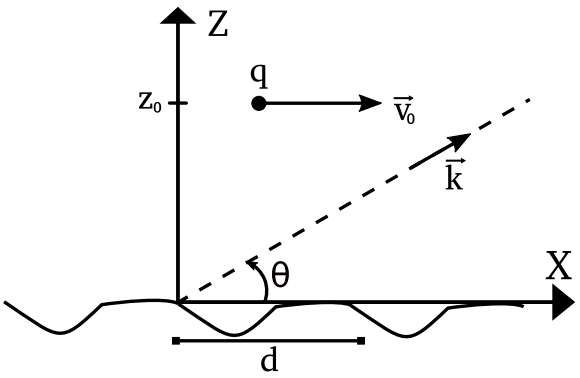

Figure 1: Smith-Purcell effect

The second model describes the charge by a set of evanescent plane waves decaying exponentially in the z direction. These waves are diffracted by the grating and give rise to the Smith-Purcell effect. The two models yield roughly to the same results, but the calculations strongly differ. The interests of the van den Berg method, that justify this work, are to allow arbitrary groove profiles, eventually made from dielectric materials, with no approximations.
When a group of electrons is considered, *coherence* effects appear, predicted identically by both models. For a bunch length shorter than the emitted wavelength the radiation is strongly enhanced. For $d \sim 1$ mm the wavelengths emitted belong to the far infrared region (THz). Smith-Purcell effect could be used as a stable electromagnetic source, along with other techniques (thermal emission, lasers) [3]. The ETALON project (Emittance Transverse And LONgitudinal) at LAL uses this radiation to get to the longitudinal profile of incident electron bunches [20], using Kramers-Kronig relations. This work deals with the opposite view: from a given longitudinal bunch profile we want to model the Smith-Purcell radiation.

Aims of the internship G. Doucas wrote a code to simulate the Smith-Purcell effect in the framework of the induced current theory. This code is called "GFW". Our objective was to initiate a new code using the grating theory to predict the effect of the surface on the Smith-Purcell radiation without the tedious calculations required by GFW. The steps of my work were then

1. Find a code to model diffraction gratings, check its correctness, understand its parameters;
2. In a simple case, adapt van den Berg's theory, find a way to connect it with the diffraction gratings theory, adapt the diffraction gratings code to the conditions of van den Berg; show that the induced currents theory and the diffraction gratings theory are not compatible;
3. Compare the "van den Berg code" with GFW.

Most of my second step's work is appended in order to ease the global readability.

1

Diffraction gratings

1.1 Definitions

1.1.1 Founding principles

Grating equation Consider a periodic surface whose groove spacing is d, and an incident monochromatic plane wave defined by its wave vector $\overrightarrow{k^i} = \frac{2\pi}{\lambda}\overrightarrow{u^i}$.

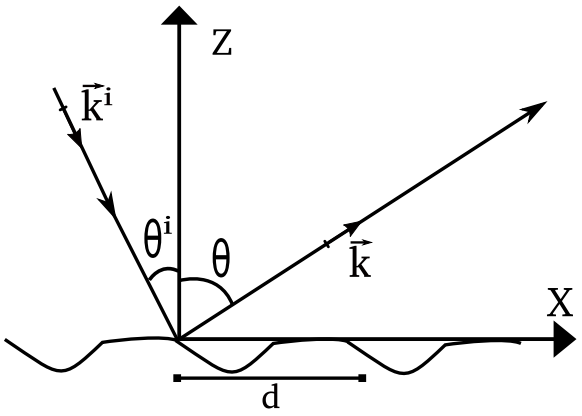

Figure 1.1: Scheme of classical diffraction grating mounting

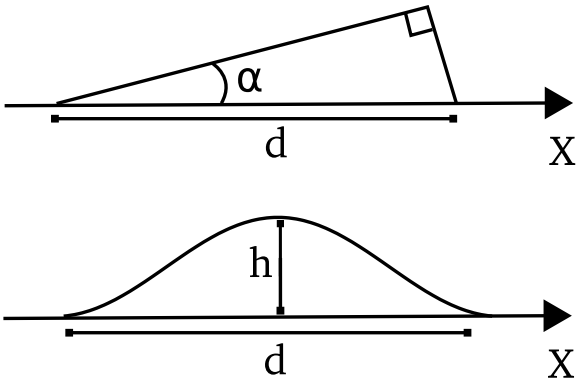

Figure 1.2: Groove profiles

Assume the incident direction lies in a plane perpendicular to the grooves and that the outgoing light is diffracted according to Fig. 1.1; the phase-matching condition implies the grating equation

$$\sin\theta^i - \sin\theta = p\frac{\lambda}{d} \tag{1.1}$$

where p is the diffraction order, $p \in \mathbf{Z}$. Other sets of angles $\{\theta_i, \theta\}$ will produce destructive interferences. Note that $\overrightarrow{k} = \left|\overrightarrow{k^i}\right| \overrightarrow{u}$ because non-linear effects of the material are neglected. The case of an incident wave outside the (x, z) plane is called *conical* diffraction.

Groove profile The profile Γ of the grooves will mainly be a right-angle triangle characterized by its blaze angle α. The interest of these *echelette* gratings is to concentrate most of the light in few orders [4]. The high h_{blaze} of these gratings is set by α according to $h_{\text{blaze}} = \frac{1}{2}d\sin(2\alpha)$. Sometimes the groove will be taken sinusoidal of depth h, as shown in Fig. 1.2. In order to have comparable grooves, we will always take $h = h_{\text{blaze}}$.

Propagation condition When θ^i is fixed, $|\sin\theta| \leqslant 1$ and Eq. 1.1 prove that there is a finite number of propagative orders. Indeed, the diffracted wavevector can be written as $k^2 = \left(\frac{2\pi}{\lambda}\right)^2$ or as $k^2 = k_x^2 + k_z^2$, which leads to $k_z = \sqrt{\left(\frac{2\pi}{\lambda}\right)^2 - k_x^2}$ with $k_x = \frac{2\pi}{\lambda}\sin(\theta)$. Then, for sufficiently large values of $|p|$, k_z is imaginary and the diffracted wave amplitude is proportional to a decaying exponential of

the z variable. The non-propagative orders are *evanescent* waves. From now on, only the propagative waves will be taken into account: to do so, the zone of interest will be restricted to the far-field region.

1.1.2 Diffraction efficiencies

Eq. (1.1) gives the directions taken by diffracted light but not the energy repartition between these directions. We introduce the incident and diffracted Pointing vectors $\overrightarrow{\Pi^i}$ and $\overrightarrow{\Pi}$. The quantity

$$\eta_p(\lambda) = \left| \frac{< \overrightarrow{\Pi} \cdot \overrightarrow{u} >}{< \overrightarrow{\Pi^i} \cdot \overrightarrow{u^i} >} \right|^2 \tag{1.2}$$

is called grating efficiency for the p-th order [6]. It depends on many parameters (see 1.2.1) but we'll mostly focus on the λ dependence.
Sometimes one can make the scalar approximation to simplify the problem. However, E.G. Loewen [4] proposed a rule of thumb for the validity of this approximation, $\frac{\lambda}{d} \leqslant 0.2$, which cannot be applied in the Smith-Purcell case, strongly linked with wave properties.

1.1.3 Polarizations

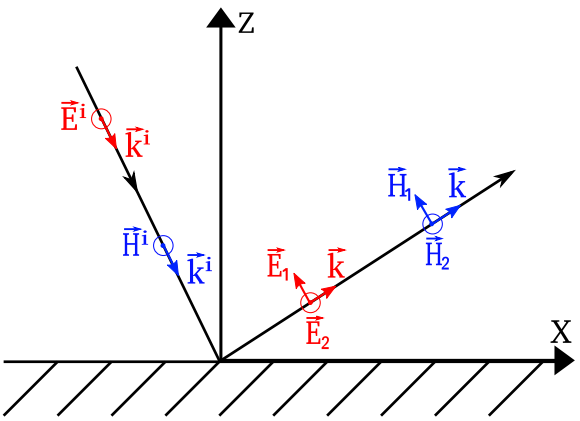

Figure 1.3: Plane preserves polarizations

Dealing with the geometry of Fig. 1.1, the more natural way to set the polarization basis is to define the Transverse Magnetic polarization ("TM", when the magnetic field is normal to the (x,z) plane) and the Transverse Electric polarization ("TE"). As an example, on Fig. 1.3, the red incident wave is TE polarized, and the blue one is TM polarized. If the incident plane is perpendicular to the grooves, an interesting property is that polarizations are preserved by the grating [4]. Consider the simple case of the specular reflection on a perfectly conducting plane as shown on Fig. 1.3. Suppose the diffracted field isn't polarized in either case, outgoing electric (respectively magnetic) field of the red (blue) wave can be decomposed in the $\{\overrightarrow{E_1}, \overrightarrow{E_2}\}$ basis ($\{\overrightarrow{E_1}, \overrightarrow{E_2}\}$). Since there is no electromagnetic field inside a perfectly conducting material, and given that the boundary conditions, we find that a plane conductor preserves polarizations ($\overrightarrow{E_1} = \overrightarrow{0}$ and $\overrightarrow{H_1} = \overrightarrow{0}$). One can adapt the specular reflection case to diffraction gratings: split the grating in slices of width dz with $dz \ll 1$, each slices being locally plane. Since changing orders only modifies diffracted directions, the argument above still applies.

1.1.4 Mountings

There are two main configurations to make use of the grating, called *mountings*.

Constant incident angle (I.A.) The first option is to keep θ^i constant and to scan the ligth intensity by varying the position of a detector that measures the output (e.g. in the θ direction).

Constant angular deviation (A.D.) The second choice is to keep the angular deviation constant. With notations of Fig. 1.1, angular deviation can be defined as the smallest angle between $-\overrightarrow{k^i}$ and $\overrightarrow{k}$. A way to carry out this mounting is to fix the angle between the source direction and the detector direction. Rotating the grating will then allow the scan. A special case is obtained when A.D. $= 0$. This configuration, called *Littrow mounting*, or *autocollimation*, is of particular interest because it gives

the larger efficiencies [4]. Some details are given in appendix A; in particular Eq. (A.3) is derived, which is useful in 1.2.3.

1.2 Simulations

1.2.1 RCWA

To model diffraction gratings, I used a code called "MRCWA" written by H. Rathgen [9] and based on the Rigorous Coupled Wave Analysis [10, 11].

Input parameters For definitions, see 1.1.

Physical parameters

1. Groove profile Γ, completely defined by $\{d, \alpha\}$ for blazed gratings and by $\{d, h\}$ for holographic gratings;
2. Incident angle θ^i, which means the mounting of MRCWA is a constant incident angle configuration;
3. Polarization of incident wave (TM or TE); according to 1.1 one can reconstruct every cases with these only two fundamental components;
4. Detector angle θ; it's linked with λ through Eq. (1.1);
5. Order p of the diffracted wave;
6. Material indices, $n_{\text{air}} = 1$ above the grating, $n_{\text{material}}(\lambda) = A(\lambda) + iB(\lambda)$ inside the grating, see 2.3.3 for a discussion, but note yet that there are two main dependences, from the nature of the material (silver, gold, multi-layered dielectric...), and the model of refractive indices.

Computational parameters

1. The number of slices N_s constituting the grating tooth, examples are shown on Fig. 1.4 and Fig. 1.5 ;

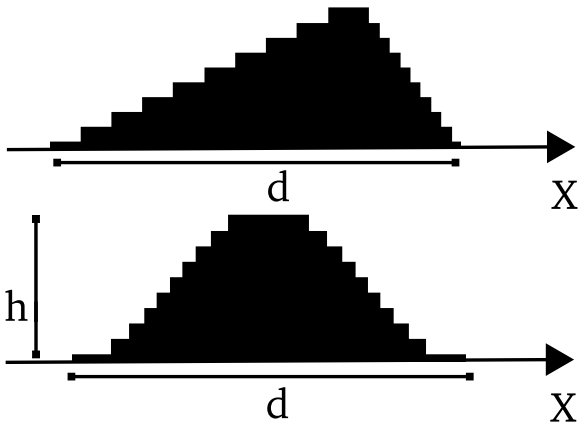

Figure 1.4: $N_{slices} = 10$, $\alpha = 30°$, $h = \frac{1}{2}d\sin(2\alpha)$

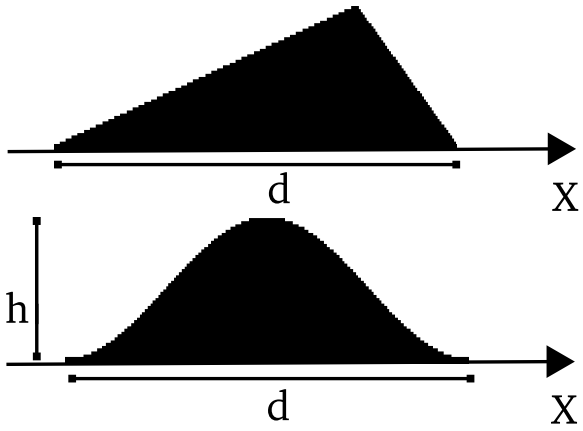

Figure 1.5: $N_{slices} = 50$, $\alpha = 30°$, $h = \frac{1}{2}d\sin(2\alpha)$

2. The number of orders N_o considered in the calculation.

Sufficient parameters It is useless to vary both d and λ since it was shown [4] that their impact on the efficiencies is identical. Then one can introduce the dimensionless parameter $\frac{\lambda}{d}$.
Sufficient input settings are then: $\{\alpha, \theta^i, \frac{\lambda}{d}$, incident polarization, p, n_{material}, N_s, $N_o\}$.
We'll use as default settings: $\{\alpha = 30°, \theta^i = 45°, 0.1 \leqslant \frac{\lambda}{d} \leqslant 2$, TM/TE, $p = 1$, n_{silver}(Drüde $\xi = 43$), $N_s = 50$, $N_o = 50\}$. An unspecified parameter is from now defined by its default value.

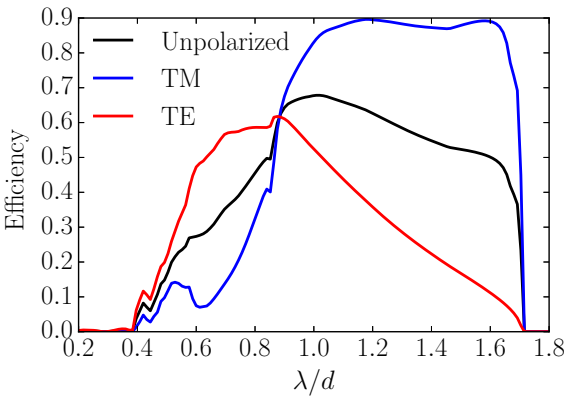

Figure 1.6: MRCWA's output with default values

Output MRCWA returns the grating efficiency (see Eq. (1.2)). A typical plot is shown on Fig. 1.6. Note that the cutoff wavelengths were already known thanks to the propagation condition (1.1.1) and Eq. (1.1). For instance the upper cutoff wavelenght is theorically $\frac{2+\sqrt{2}}{2} \approx 1.7$.

1.2.2 Convergence study

Number of slices When the number of slices N_s is sufficiently large, the quality of the output increases but the calculation time does too. This time roughly grows linearly as N_s increases. Giving the default input parameters to MRCWA, but varying N_s, we obtain Fig. 1.7. Without defining a more precise norm to quantify the convergence, we'll admit for now on that $N_s = 100$ is a sufficient division of the tooth.

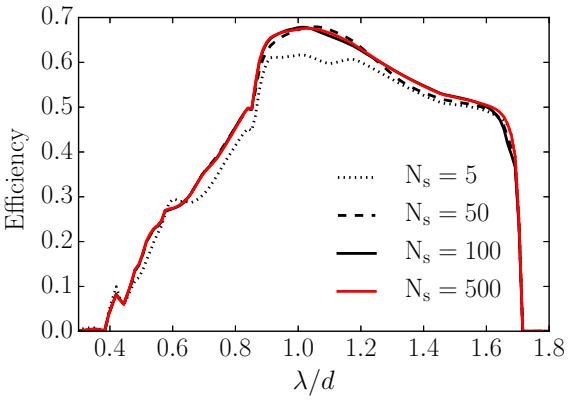

Figure 1.7: Convergence of the number of slices taken into account by MRCWA

Number of orders The default value is $N_o = 50$. J.J. Hench has shown [11] that with such N_o the absolute approximation error is less than 10^{-4} (the reference is a calculation with $N_o = 100$).

1.2.3 Physical checks

Before any attempt to use MRCWA in a Smith-Purcell context, I wanted to check its correctness as well as my understanding of diffraction gratings. I used some manufacturers' experiments to compare with MRCWA's data. I also took advantage of three physical criteria, *energy conservation*, so called *Rayleigh anomalies*, and the *reciprocity theorem*.

Littrow mounting Diffraction gratings have numerous applications (spectroscopy, compression of a laser's pulse, X-ray crystallography...), their performance when one of the input parameters is changed has been widely studied [4, 5, 6]. Moreover gratings are commercialized for a long time. Thorlabs for instance provides *measured* efficiency curves for each type of grating they sell [23]. Such data is shown on Fig. 1.8 with the following set of input parameters: $\{\alpha = 26.5°$, $d = 0.83$ μm, Littrow mounting, 0.2 $\mu\text{m} \leqslant \lambda \leqslant 1.66$ μm, $p = 1$, $n_{\text{Al}}\}$. MRCWA shows good comparison. According to the definition of the Littrow mounting 1.1.4 and to Eq. (A.3), I set MRCWA input parameters such as: $\{\alpha = 26.5°$, $d = 0.83$ μm, $\theta^i = \arcsin\left(\frac{\lambda}{2d}\right)$, 0.2 $\mu\text{m} \leqslant \lambda \leqslant 1.65$ μm, n_{Al}(Rakić 1998)$\}$. As an exception, the data is plotted as a function of λ and not of λ/d, in order to keep the original curves from Thorlabs. The grating period is then reintroduce; its value $d = 0.83$ μm isn't randomly chosen: indeed it's equivalent to an integer *groove frequency* of 1200 gr/mm. This time, the upper cutoff wavelength is given by Eq. (A.2), i.e. $\lambda_{\max} = 2d \approx 1.66$.

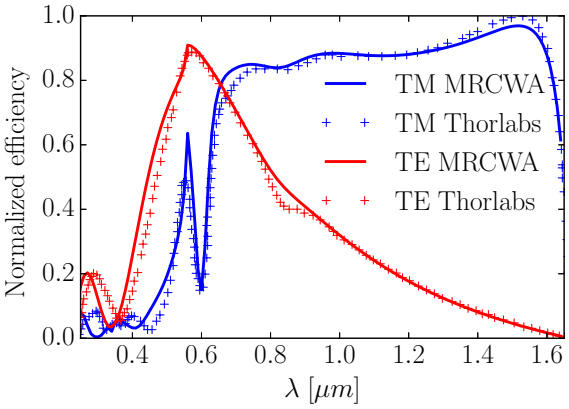

Figure 1.8: Comparison between MRCWA simulations and experimental measures

Wood's anomalies Some strange performances, called *Wood's anomalies* [7], can be observed when an order appears or disappears. Evanescent waves becoming propagative (or the contrary) because of the critical change of a grating parameter (for instance θ^i or $\frac{\lambda}{d}$). If one plots the map of the efficiencies as a function of θ^i and $\frac{\lambda}{d}$, some corresponding lines should be seen. This lines are given by the propagation condition (cf. 1.1.1) and are plotted on Fig. 1.10 with $m \in [\![1, 4]\!]$. In order to keep the information about the polarization, I chose to plot the degree of polarization (D.O.P.) defined as

$$DOP = \frac{\eta_{\text{TE}} - \eta_{\text{TM}}}{\eta_{\text{TE}} + \eta_{\text{TM}}} \tag{1.3}$$

For example, when there is only TE polarization, $DOP = 1$ and a blue color is shown. Black color stands for unpolarized light. It's important to keep in mind that this map only deals with the performance of the first order, although the anomalies are due to orders for which $p \neq 1$.

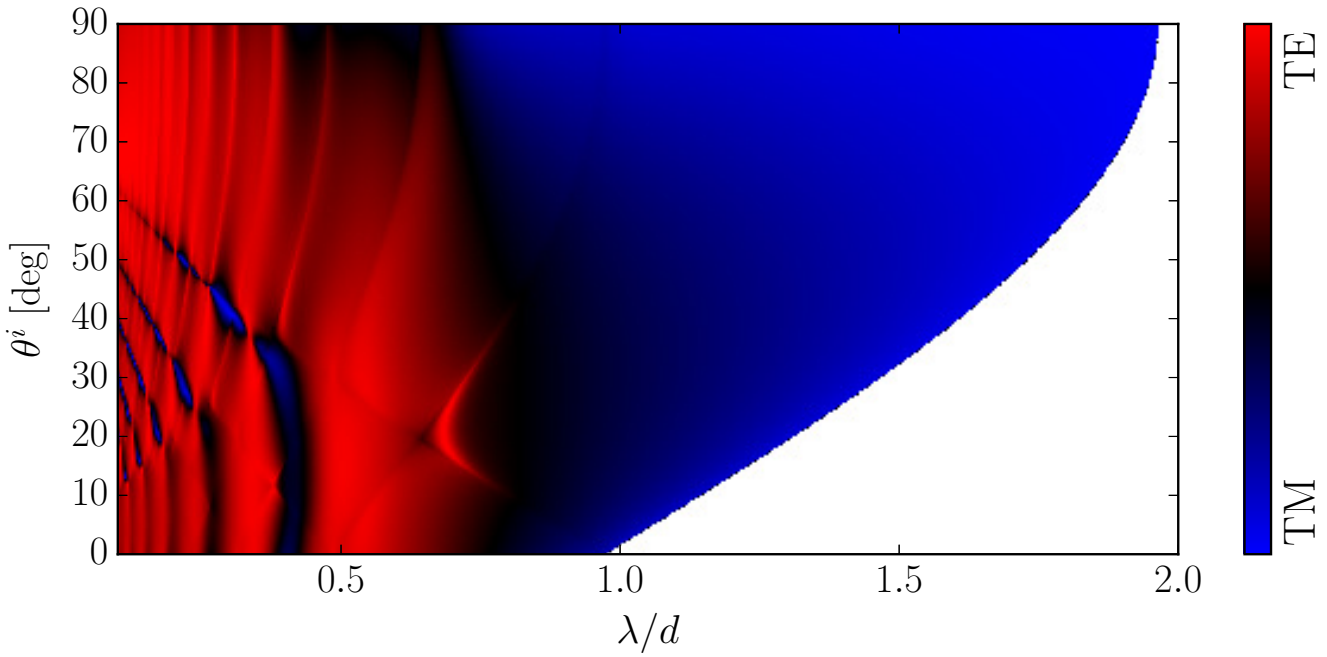

Figure 1.9: Map of the DOP with default parameters

Reciprocity theorem Theory [8] predicts that efficiencies remain the same when angles of incidence and diffraction are exchanged. Other parameters being set, if light comes under an incidence of θ_1^i, the diffracted angle is $\theta_1 = \arcsin\left(\sin\theta_1^i - \lambda/d\right)$. Now set as input parameter $\{\theta^i = -\theta_1\}$: the efficiency is supposed to remain constant. This result is called the *reciprocity theorem*. On Fig. 1.9 one should see a *vertical* symmetry (keep constant λ/d) along the line defined by the coordinates $\left(\lambda/d, \arcsin\left(\frac{\lambda}{2d}\right)\right)$. The symmetry is easier to note in the plane $(\lambda/d,\ \sin\theta^i)$ where it's marked by a line of slope $\frac{1}{2}$, see Fig. 1.10.

Energy conservation As a first approximation, one could neglect losses due to the material (which could be supposed perfectly reflective). Therefore, energy conservation states that the incident energy

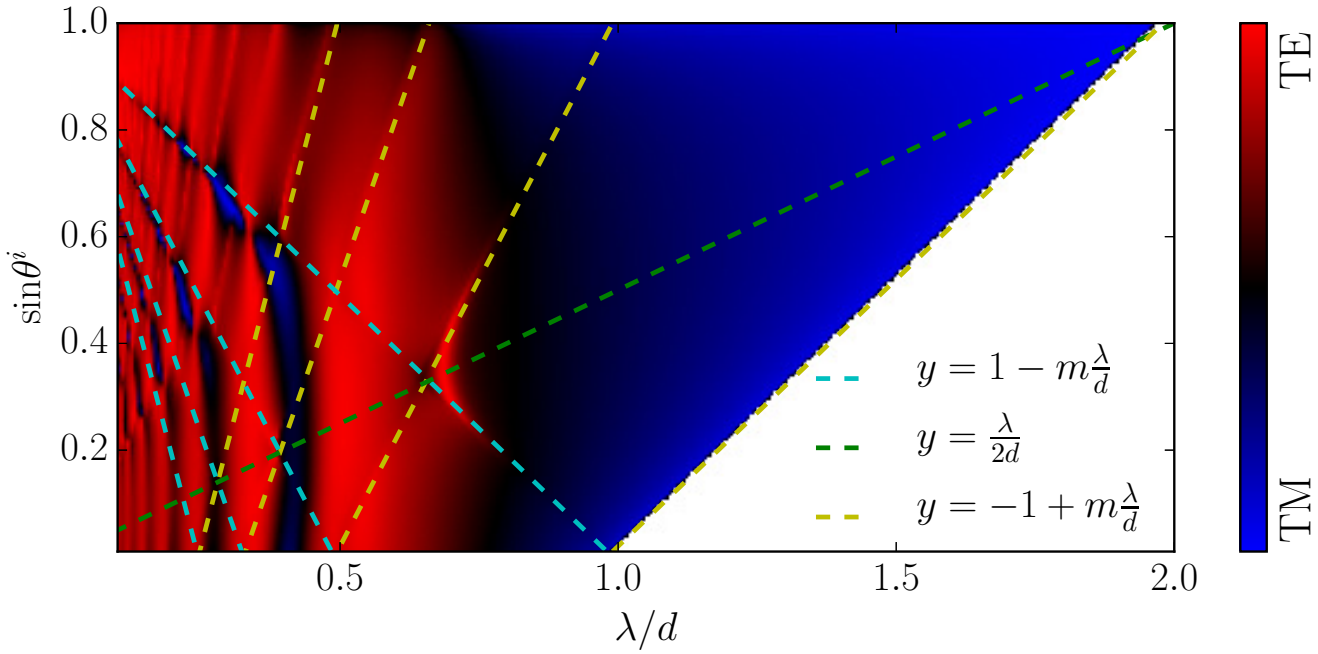

Figure 1.10: Map of the DOP highlighting the reciprocity theorem and Wood's anomalies

is totally divided between diffracted orders. With default values (Fig. 1.6), apart from setting $\{\lambda/d = 1,\ \text{TM}\}$, one can show with the grating equation that the only diffracted orders are the specular order ($p = 0$) and the first order. Yet with MRCWA the corresponding sum of the efficiencies only comes to $\sum_p \eta_p \approx 0.88$. This property won't be fulfilled without considering *transmitted* orders. Such a study is beyond the scope of my objectives.

1.2.4 Grating defaults

The manufacture of gratings isn't perfect. Figs. 1.11, 1.12 show examples of gratings produced at LAL, for typical periods of $d \sim 1$ mm. The precision of manufacturers is here around 100 μm, sometimes 10 μm. One can see that for the gratings presented, anomalies aren't negligible, and would likely modify the grating efficiencies. Since these defaults are regular, one could predict their impact on the efficiencies when coding the tooth's profile on MRCWA (cf. 1.2.1).
The gratings that I'll consider in the following sections has a period $d \sim 8$ mm; thanks to the precision of manufacturers, I'll suppose as a first approximation that the consequences of anomalies are only minor corrections, and won't study them. However, we'll see in 3.3 that the flexibility of MRCWA could be useful with the Smith-Purcell radiation emitted by very short electron bunches.

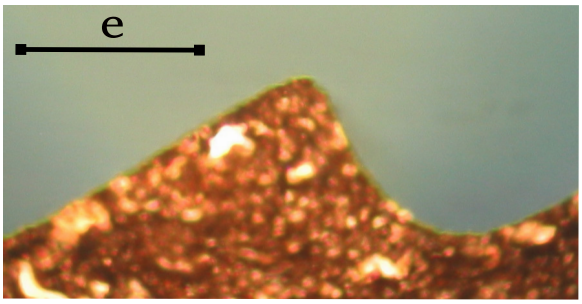

Figure 1.11: Wire eroded aluminium tooth, $e = 0.3$ mm

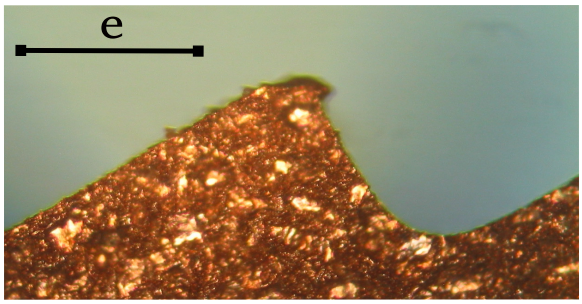

Figure 1.12: Milled aluminium tooth, $e = 0.4$ mm

2

Single electron case: Smith-Purcell radiation

Before considering the real case of an electron bunch, we need to investigate first the nature of the radiation emitted by a single electron passing over a periodic structure. We want to know if one model of the Smith-Purcell radiation is compatible with the previous study of gratings.

2.1 Van den Berg's model

In this approach, Smith-Purcell radiation is caused by the diffraction of evanescent waves on the grating. I adapted (appendix B) the equations from van den Berg and Haeberlé [12, 17, 18] when the detector belongs to the incident plane. The relativistic electron can be described with a set of evanescent plane waves (cf. B.1). If $z_0 \sim \lambda_e$ (cf. Fig. 1 and Eq. (B.19)), the material can perturb the evanescent field and give rise to propagative waves. In the Smith-Purcell case, the incoming waves are diffracted by a grating, but this approach is of general validity and also explains for instance the Cherenkov effect [13] (refraction of incoming evanescent waves).

2.1.1 Spectrum

According to the far-field approximation, the diffracted evanescent waves are not taken into account in the calculation of the Smith-Purcell radiation. For such orders, it is possible to define a diffraction angle θ_n (see Fig. 1, $\theta_n \equiv \theta$), $\theta_n \in [0, \pi]$, such as

$$\begin{cases} \alpha_n = k_0 \cos\theta_n \\ \theta_n = k_0 \sin\theta_n \end{cases} \tag{2.1}$$

Using Eqs. (B.11), (2.1), introducing $\beta = \frac{v_0}{c}$, it follows

$$\lambda = \frac{d}{-n}\left(\frac{1}{\beta} - \cos\theta_n\right) \tag{2.2}$$

The integer $n \in \mathbf{Z}$ in Eq. (2.2) is called *order* of the Smith-Purcell radiation, and is analogous to p in classical diffraction (Eq. (1.1)). In B.3, I show that using recent experiments at CLIO [20] as reference data, $\lambda \sim 1$ mm, $d \sim 8$ mm, $E \sim 50$ Mev, orders of magnitude for n are: $-16 \leqslant n \leqslant -1$.

2.1.2 Radiated energy

Assume the geometry of Fig. 1, from B.5, the energy per angle radiated in the θ direction due to one electron can be written as

$$\left.\frac{\partial W_n}{\partial\theta}\right|_1 = \frac{q^2 n^2}{8\pi\epsilon_0 d} \frac{\sin^2\theta}{\left(\frac{1}{\beta} - \cos\theta\right)^3} |R_n|^2 \exp(-\frac{z_0}{\lambda_e}) \tag{2.3}$$

Note that $|R_n|^2$ is in principle different from $|R'_n|^2$ calculated in the framework of induced currents model (cf. 2.4 for comparison). An other significant change is the $\sin^2\theta$ factor: it will smooth the curve.

2.2 Induced currents model

According to the induced currents model [14, 15], the incoming charge induces a current on the grating [2]. Each groove radiates the same field: Smith-Purcell radiation is caused by interferences between those sources (same result as Eq. (2.2)). h being defined on Fig. 1.2, the angular distribution of energy for the n-th order is given by [21]

$$\left.\frac{\partial W'_n}{\partial \theta}\right|_1 = \frac{q^2 n^2}{2\epsilon_0 d} \frac{1}{\left(\frac{1}{\beta} - \cos\theta\right)^3} \left|R'_n\right|^2 \exp\left(-\frac{z_0 + h}{\lambda_e}\right) \tag{2.4}$$

with $|R'_n|^2 = \left|\overrightarrow{u_n} \times \left(\overrightarrow{u_n} \times \overrightarrow{G}\right)\right|^2$, $\overrightarrow{G}$ being defined from the Fourier transform of the induced current vector. In comparison with Eq (2.3), the important result is that $|R'_n|^2$ depends on the electron energy [15]. Therefore, we can't use the grating code MRCWA to generalise the induced currents model. However, I take advantage here of this model to draw an analogy between the order n of the Smith-Purcell radiation, and the diffraction order p. Indeed both integers quantify a new mode of constructive interferences; from now on I'll consider that $n \equiv p$.
To simulate $|R'_n|^2$, I used "GFW", a code written by G. Doucas [15]. The sufficient input parameters are: $\{\alpha_{\text{blaze}}, \frac{\lambda}{d}, \phi, \gamma, n\}$. γ is the Lorentz term, in which the energy dependence is included. ϕ is the angle between the emitted wave and the plane of incidence. In this report, we've supposed that $\phi = 0$.

2.3 Using MRCWA in a Smith-Purcell context

We show in B.4 that the $|R_n|^2$ factor of the van den Berg's model is nothing more than the grating efficiency η_p, which is known thanks to MRCWA. The evanescent nature of incident waves won't invalidate the analogy, which was an initial concern. A question remains: how input parameters $\{\alpha$, θ_i, $\frac{\lambda}{d}$, incident polarization, p, n_{material}, N_s, $N_o\}$ should be adapted? Some are easy to transpose $\{\alpha$, $\frac{\lambda}{d}$, N_s, $N_o\}$, but the others deserve discussions.

2.3.1 Order

According to 2.2, one can consider that $n \equiv p$ is shown. Then, the arguments that led us to restrict the diffraction study to $p = 1$ still apply. The higher the order is, the smaller the range of emitted wavelengths is (cf. B.3 for a proof). Moreover, the intensity diffracted tends to decrease for high orders. Then, we will focus on the first order, for which $n = -1$.

2.3.2 Grazing incidence

A major difficulty of a "van den Berg code" based on a "classical diffraction code" is that incident waves are not propagative in the case of Smith-Purcell radiation. With notations of Fig. 1.1, the angle of incidence would be $\theta^i = 90$ degrees, since the waves are propagative in the x direction and are evanescent in the z direction. Such an angle can't be rigorously entered in MRCWA. However, the Smith-Purcell relation and the grating equation are very similar when considering high energetic electrons for which $1/\beta \approx 1$. In such case, with $\sin\theta^i \approx 1$

$$\frac{\lambda}{d} \approx \begin{cases} \frac{1}{n}(1 - \cos\theta_a), \text{ Smith} - \text{Purcell radiation} \\ \frac{1}{p}(1 - \sin\theta_b), \text{ grating equation,} \end{cases} \tag{2.5}$$

Moreover, $\cos\theta_a = \sin\theta_b$ because conventions are different in each case: for Smith-Purcell radiation (Fig. 1), $\theta_a \in [0, \pi]$, and for the grating equation (Fig. 1.1), $\theta_b \in [-\pi/2, \pi/2]$. We also know that $n \equiv p$. Therefore, this unrigorous argument is in agreement with the previous physical idea. In the following work, I'll enter $\theta^i = 89.9°$ in MRCWA, and will name this assumption the "optical hypothesis".

2.3.3 Refractive indices

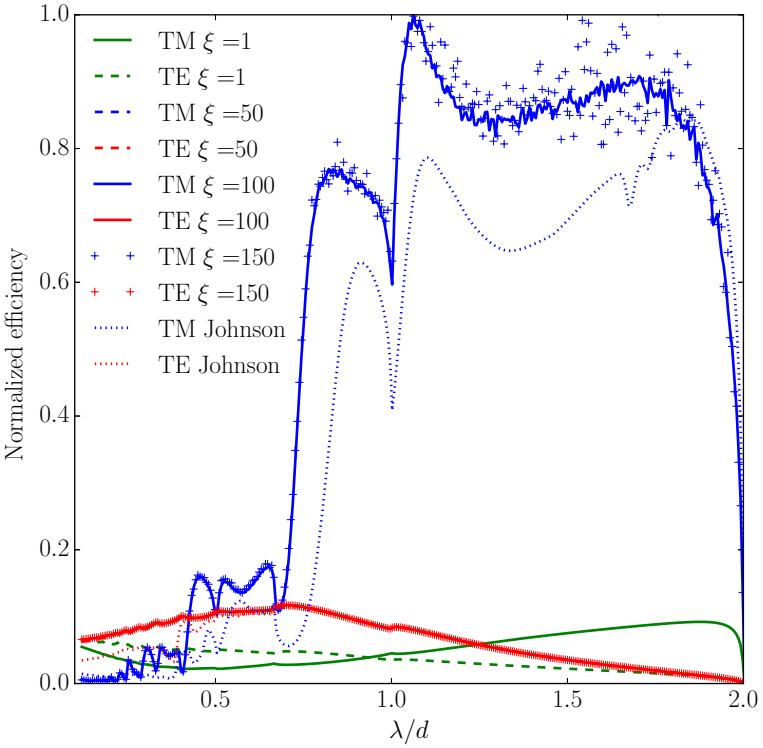

Figure 2.1: Extension to far infrared region

The material used at CLIO is aluminium [20], but we'll use silver as reference material. The differences between these two metals are negligible at our wavelengths range. We have already explained in 1.2.1 that the relevant variable to describe gratings was λ/d. However, there remains an implicit dependence in λ through the performance of the material. This dependence is included in the refractive indices $n_{\text{silver}}(\lambda) = A(\lambda) + iB(\lambda)$, A and B ruling respectively dispersion and absorption.
The evolution of $n_{\text{silver}}(\lambda)$ isn't obvious at all, although the reflectance defined by the Fresnel equation $R = \left|\frac{n_{\text{silver}}-1}{n_{\text{silver}}+1}\right|^2$ (in normal incidence for unpolarized light) approximately equals one for $\lambda \gg 500$ nm [4]. We are interested now in the far infrared region. Unfortunately, most of the studies of diffraction gratings deal with incoming wavelengths around the micrometer; at this order of magnitude of wavelength, many works have been done to list the evolution of the material refractive indices (e.g. Johnson [19], 0.188 μm $\leqslant \lambda \leqslant$ 1.937 μm). But none of these studies tackle the millimetre range, which is the most important for the Smith-Purcell effect in our case. Therefore, we have to model it.

Drüde model In a non-magnetic, homogeneous, linear, isotropic metal, consider that the movement of the electrons is ruled by a damped harmonic oscillation (Lorentz model) where the damping factor is $1/\tau$, τ being the time constant between two collisions "electron/atom". Consider now a free electrons gas for which the resonance frequency equals zero (Drüde model). Add an other hypothesis: $\lambda \gg 2\pi c\tau$. Then one can obtain [3]

$$n_{\text{metal}} = (1+i)\xi_1\sqrt{\lambda} \tag{2.6}$$

where $\xi_1 = \sqrt{\dfrac{\sigma}{4\pi\epsilon_0 c}}$ and σ is the metal conductivity.
In the case of silver [22]: $\tau \approx 2.3 \times 10^{-13}$ s, $\sigma \approx 63 \times 10^6$ S.m^{-1}, $\xi_1 \approx 4.3 \times 10^4$ m$^{-1/2}$.
Thus Eq. (2.6) is valid if $\lambda \gg 400$ μm. The Drüde model can be used in good approximation for $\lambda \geqslant 1$ mm, and one can see on Fig. 2.1 that the Johnson lines are not far from the Drüde curves. Then I'll use the Drüde model for 0.1 mm $\leqslant \lambda \leqslant$ 20 mm.
I define ξ as $\xi_1 \times 10^{-3}$. On Fig. (2.1) I've plotted the output of MRCWA in grazing incidence, when the law of n_{silver} follows Eq. (2.6), for $\xi \in \{1, 50, 100, 150\}$, and when it's defined by Johnson's measures. The efficiencies are normalized upon $\xi = 150$. There is no huge differences between $\xi = 50$ and $\xi = 100$, but for $\xi > 100$ the output begins to be more and more perturbed by noise. From now on we'll enter in MRCWA: $n_{\text{silver}} = (1+i)\sqrt{\lambda} \times 4.3 \times 10^4$.

2.3.4 Polarization

Thanks to the work done in B.1, we know that Smith-Purcell radiation is TM polarized in the plane of incidence. From now on the corresponding input parameter will always be TM.

2.4 Comparison of grating factors R^2

Now that MRCWA input parameters have been modified to fit with a Smith-Purcell context, we are able to compare $|R'_n|^2$ from the induced currents model and $|R_n|^2$ from the van den Berg's model. As a reminder:

$$\left.\frac{\partial W_n}{\partial \theta}\right|_1 = \begin{cases} \alpha \left|R'_n\right|^2, \text{ induced currents} \\ \beta \left|R_n\right|^2 \sin^2\theta, \text{ van den Berg} \end{cases} \tag{2.7}$$

From Eqs. (2.4) and (2.3) one can be convinced of $\alpha \sim \beta$. Their differences won't be studied, I will consider that these two terms are equal. To simulate $|R'_n|^2$, I used GFW (cf. 2.2) with the following input parameters: $\{\alpha_{\text{blaze}}, 0.1 \leqslant \frac{\lambda}{d} \leqslant 2, \phi = 0, \gamma = 100, n = -1\}$.

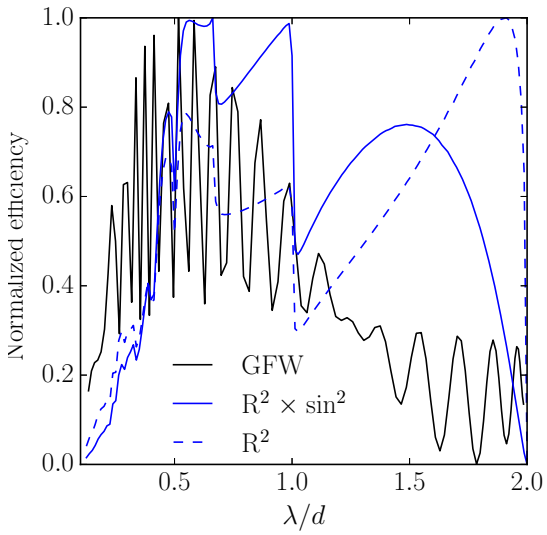

Figure 2.2: Radiation factors, $\alpha_{\text{blaze}} = 15°$

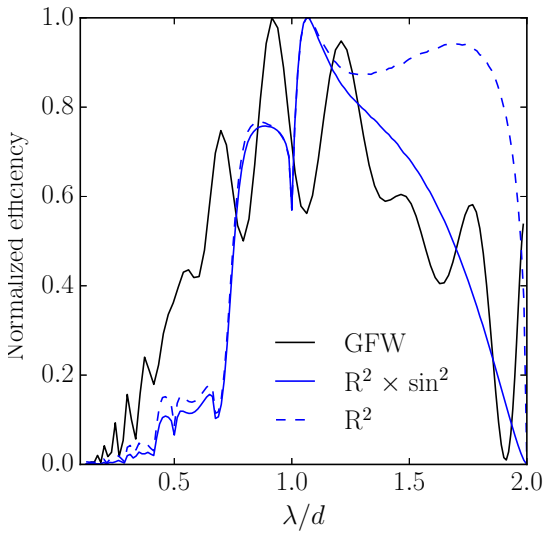

Figure 2.3: Radiation factors, $\alpha_{\text{blaze}} = 30°$

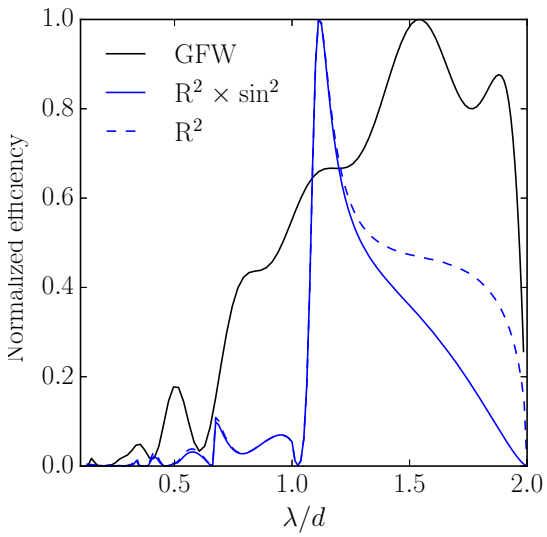

Figure 2.4: Radiation factors, $\alpha_{\text{blaze}} = 45°$

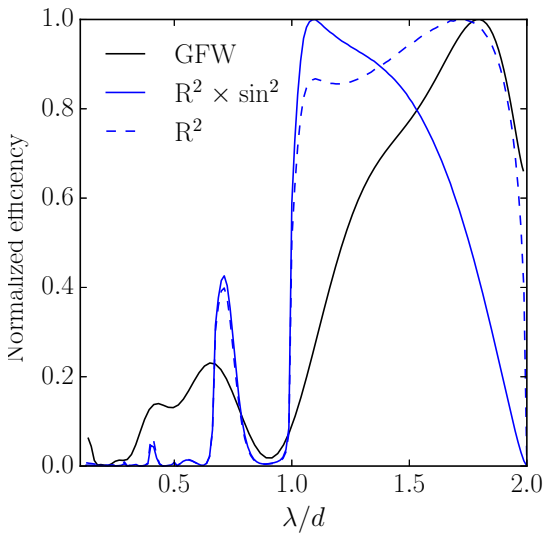

Figure 2.5: Radiation factors, $\alpha_{\text{blaze}} = 60°$

Figs. 2.2, 2.3, 2.4, 2.5 show a comparison between $|R'_n|^2$ (called GFW), $|R_n|^2$ (called R^2) and $|R_n|^2 \sin^2\theta$ (called $R^2 \times \sin^2$), for $\alpha_{\text{blaze}} \in \{15, 30, 45, 60\}$, others parameters being set as explained in 2.3.

The conversion from the diffracted angle θ and λ/d is given by Eq. (2.2). Each curve is normalized

independently from the others.
Note that the smaller α_{blaze} is, the more oscillations GFW outputs. This performance has no physical explanations, and could be explained by a wrong treatment of the Fourier transforms in GFW. Apart from this point, the codes have similar results; the particular case of $\alpha_{\text{blaze}} = 45°$, which give very different results, isn't understood yet. Therefore, at this stage, it is uncertain to say for good which code better models the Smith-Purcell radiation. In this regard, planned experiments at CLIO will soon return a verdict.
Besides, an important point is that GFW also predicts an extinction of the TE component of polarization: the corresponding black curves of previous figures are relative to TM polarization, just like the ones given by MRCWA, in blue. However, in practice, a TE's extinction has never been completely observed in the experimental "plane of incidence". Indeed, the detectors used to measure Smith-Purcell radiation at CLIO are characterized by a non-zero angular aperture. In order to fit with the experimental mounting, the theoretical data must be obtained after a step of integration over ϕ, e.g. $\phi = \pm 5$ degrees. Moving detectors away from the grating would of course solve the problem, but it would also cause a decrease of the signal's intensity, and by the way the experimental facilities available don't have this possibility. Thus, detectors with a small angular aperture are going to be used at CLIO soon, with for example $\phi = \pm 1$ degrees. In fact, the van den Berg calculations could also be done for $\phi \neq 0$, yet more tedious in such case; the underlying theory is called *conical* diffraction.

2.5 Single electron yield

Using Eq. (2.3), we can now plot (Fig. 2.6) the energy per angle radiated by one electron through the Smith-Purcell effect (the exponential term is neglected). The conversion $\lambda/d \to \theta$ is given by Eq. (2.2).

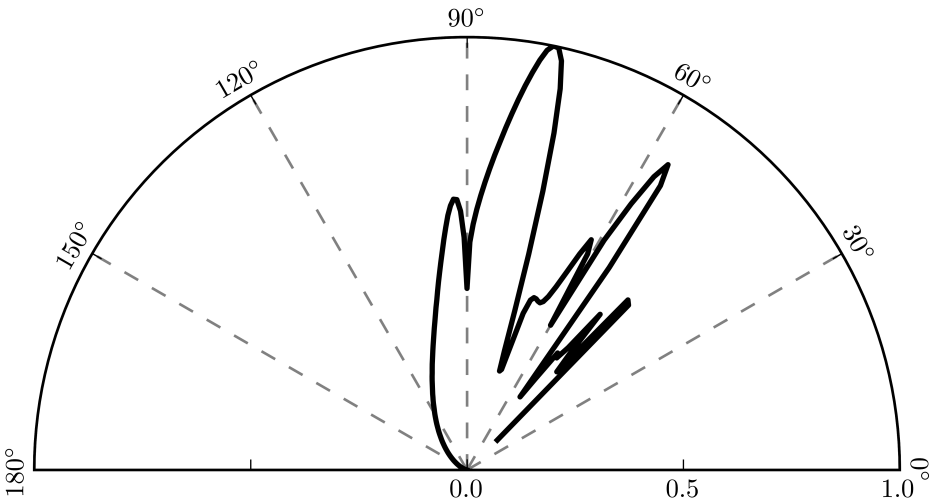

Figure 2.6: Normalized single electron radiation

3

Electron bunch case: coherent Smith-Purcell radiation

Now we consider a *bunch* of N_e electrons passing over the grating. If the electrons are taken independent (no group behaviour), the charge density can be factorized as [15]

$$\rho(t = x/v_0, y, z) = qT(t)K(y, z) \tag{3.1}$$

where $K(y, z)$ denotes the transverse distribution of the bunch, and T is the longitudinal bunch profile. K doesn't interest us and we won't try to calculate it (see [21] for details).

3.1 Longitudinal profile of electron bunch

In order to simulate the Smith-Purcell radiation, we need to set a longitudinal profile. We choose to model T as an asymmetric Gaussian, with parameters FWHM $\in \{2.5, 5, 7.5\}$ ps, $\epsilon = 0.5$ (see appendix C for definitions). Call $\widetilde{T}(\lambda)$ the Fourier transform of T; they are plotted on Figs. 3.1, 3.2.

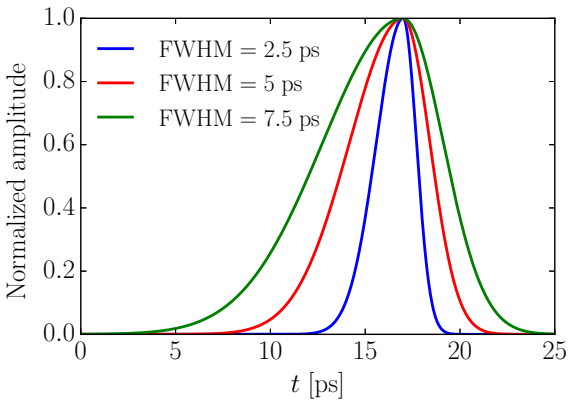

Figure 3.1: Longitudinal profile T

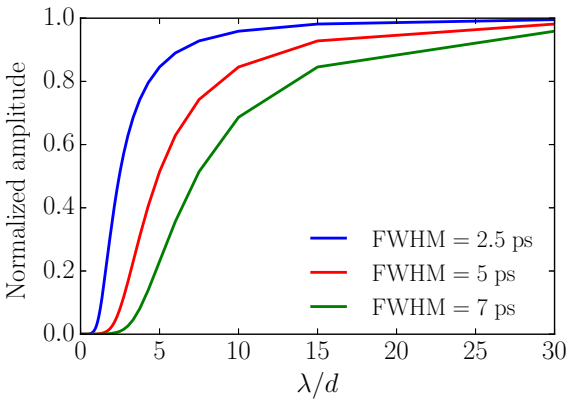

Figure 3.2: Fourier transform amplitude of T

3.2 Coherence effects

According to [15], the yield for N_e electrons is:

$$\left.\frac{\partial W_n}{\partial \theta}\right|_{N_e} = \left.\frac{\partial W_n}{\partial \theta}\right|_1 \left(N_e K_1 + N_e^2 K_2 \left|\widetilde{T}(\lambda)\right|^2\right) \tag{3.2}$$

K_1, K_2 two constants which depend on the transverse profile; the key point is that K_1, K_2 are independent from λ. We'll admit that $N_e^2 K_2 \gg N_e K_1$ for $N_e \gg 1$. Then, if λ is sufficiently high (call $\lambda_{\min}$ the critical value), the second term in Eq. (3.2) prevails over the first one. Because of the properties of the Fourier transform, one can obtain that $\Delta\nu \times \text{FWHM} \sim 1$ which can be rewritten as $\lambda_{\min} \sim c \times \text{FWHM}$. If l_{bunch} denotes the electron bunch length, we see that *coherent* radiation is emitted for $\lambda > l_{\text{bunch}}$. Such radiation is strongly enhanced compared to the term $N_e K_1$, therefore it's easier to measure. But more importantly Kramers-Kronig relations can permit a derivation of T from $\left|\widetilde{T}(\lambda)\right|^2$.

3.3 Coherent Smith-Purcell radiation spectrum

According to what has just been said, the energy per angle radiated by an electron bunch in the θ direction is simply proportional to the product between the single electron yield given in 2.5 and the Fourier transform amplitude of T plotted on Fig. 3.2:

$$\left.\frac{\partial W_n}{\partial \theta}\right|_{N_e} \propto \left.\frac{\partial W_n}{\partial \theta}\right|_{1} \times \left|\widetilde{T}(\lambda)\right|^2 \tag{3.3}$$

This work is presented on Fig. 3.3.

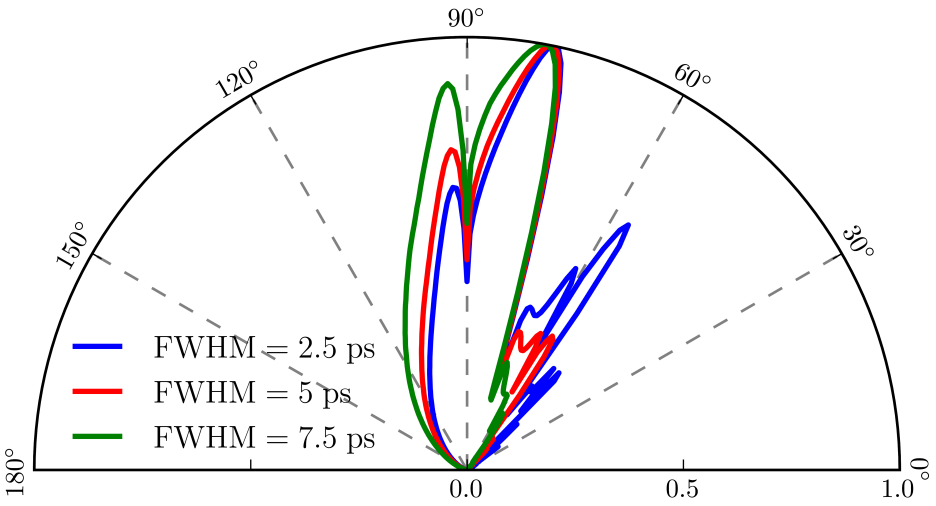

Figure 3.3: Normalized angular distribution of coherent Smith-Purcell radiation

One can observe that the smaller the bunch is, the more the distribution is shifted towards small wavelengths (small angles). If FWHM becomes lower than 1 ps, it's reasonable to change the grating period d, to counterbalance this shift. At the FACET User Facility at SLAC during the E-203 experiment [16], for bunches of 1 ps long, the smallest period of the gratings was $d = 50$ μm. At this range of periods, defaults are more easily present 1.2.4. For such bunches, the flexibility of the van den Berg code would be a useful advantage over GFW's method.

Conclusion

During my internship, I've set up a code to simulate Smith-Purcell radiation while using the computing power of diffraction gratings' simulations. This idea can't be applied to the induced currents theory, but fits naturally with the model developed by P. M. van den Berg. At the same time, it was necessary to understand, adapt and reference arguments justifying this approach. I restricted my work to the simple case of normal incidence, and for emitted radiations that belong to the incidence plane. A limitation of this code is that the grating is considered of infinite width; the consequences of such hypothesis have not been studied.
This work allows an extension to dielectrics and to arbitrary profiles. This is useful when one wants to predict the changes due to the grating's defaults. It could also open the way to a systematic study in optimizing grating parameters, in order to know for instance which blaze angle produces the best yield of Smith-Purcell radiation at a specific wavelength. An other useful work would be to predict *absolute* intensities that detectors should measure; this report only presented normalized repartitions of energy. With notations of Eqs. (2.7), it involves to take into account α and β.
An extension to the pre-wave zone is possible, yet far beyond this work.
But the essential upgrade needed right now would be to take into account emitted radiations out of the plane of incidence. Such improvement would make the van den Berg code as operational as GFW. Fortunately, the grating problem on which the calculations would be based is also resolved. Indeed, the RCWA method remains available for conical diffraction. Although MRCWA of H. Rathgen would be insufficient, a free software originally written by B. Dhoedt and named "RODIS" [24, 25] implements such tasks. Coming experiments at CLIO are expected to confirm or disprove the van den Berg code's results.

Thanks

I would like to warmly thank Nicolas Delerue, my supervisor during this internship, and Stéphane Jenzer, engineer for the ETALON project. There help has been decisive during the daily work, and during the preparation of this report. I also would like to thank the other students of the group for their advices and good company: Anne-Fleur, Geoffrey and Yu.

A

About Littrow mounting

In constant A.D. configuration, rotating the grating allows the scan according to Eq. (1.1) rewritten as

$$\sin\left(\theta^i - \frac{A.D.}{2}\right)\cos\left(\frac{A.D.}{2}\right) = \frac{p\lambda}{2d}, \tag{A.1}$$

where θ^i now represents the rotation angle of the grating.
Note that in Littrow mounting for which $A.D. = 0$, Eq. (A.1) becomes much simpler:

$$\sin\theta^i = \frac{p\lambda}{2d}, \tag{A.2}$$

In the constant A.D. case, setting λ amounts to set θ^i, which is not true for the constant I.A. case. All other parameters being fixed, it implies that η_{ad} (the efficiency with constant A.D.) is only a function of λ while its equivalent η_{ia} is a function of λ and θ^i. This will be of practical interest in 1.2.3, when we will use a constant I.A. code (MRCWA) to extract constant A.D. curves. Indeed, in the special case of a Littrow mounting, if one knows $\eta_{\text{ia}}\left(\lambda, \theta^i\right)$, one can derive $\eta_{\text{ad}}\left(\lambda\right)$ with the following formula

$$\eta_{\text{ad}}\left(\lambda\right) = \eta_{\text{ia}}\left(\lambda, \arcsin\left(\frac{p\lambda}{2d}\right)\right) \tag{A.3}$$

B

Calculations around van den Berg model

B.1 Incident field

Suppose the geometry of Fig. 1.1 and let an electron pass through the periodic structure with a velocity $\overrightarrow{v} = v_0\overrightarrow{i_x}$ at $z = z_0$ [17]. The electron can be represented by a set of Fourier integrals

$$\overrightarrow{E^i}(x,z,t) = \frac{1}{2\pi}\int_{\mathbf{I}} d\omega \widetilde{\overrightarrow{E^i}}(x,z,\omega), \tag{B.1}$$

$$\overrightarrow{H^i}(x,z,t) = \frac{1}{2\pi}\int_{\mathbf{I}} d\omega \widetilde{\overrightarrow{H^i}}(x,z,\omega). \tag{B.2}$$

Only positive frequencies have a physical meaning: $\mathbf{I} = \mathbf{R_+}$. A similar expression can be written for the electric-current density. If q is the electron charge then $\overrightarrow{J}(x,z,t) = qv_0\delta(x - v_0t, z - z_0)\overrightarrow{i_x}$ and $\widetilde{\overrightarrow{J}}(x,z,\omega) = qv_0\delta(z - z_0)\exp(i\alpha_0 x)\overrightarrow{i_x}$ where $\alpha_0 = \frac{\omega}{v_0}$. The Fourier transforms of the fields satisfy the Maxwell equations

$$\begin{cases} \overrightarrow{\nabla} \times \widetilde{\overrightarrow{H^i}} + i\omega\widetilde{\overrightarrow{E^i}} = \widetilde{\overrightarrow{J}} \\ \overrightarrow{\nabla} \times \widetilde{\overrightarrow{E^i}} - i\omega\widetilde{\overrightarrow{H^i}} = \overrightarrow{0} \end{cases} \tag{B.3}$$

Expanding Eq. (B.3) in Cartesian coordinates yields to uncoupled systems

$$\begin{cases} \dfrac{\partial \widetilde{H_x^i}}{\partial z} - \dfrac{\partial \widetilde{H_z^i}}{\partial x} + i\omega\epsilon_0 \widetilde{E_y^i} = 0 \\ -\dfrac{\partial \widetilde{E_y^i}}{\partial z} - i\omega\mu_0 \widetilde{H_x^i} = 0 \\ \dfrac{\partial \widetilde{E_y^i}}{\partial x} - i\omega\mu_0 \widetilde{H_z^i} = 0 \end{cases} \tag{B.4}$$

$$\begin{cases} \dfrac{\partial \widetilde{E_x^i}}{\partial z} - \dfrac{\partial \widetilde{E_z^i}}{\partial x} - i\omega\mu_0 \widetilde{H_y^i} = 0 \\ -\dfrac{\partial \widetilde{H_y^i}}{\partial z} + i\omega\epsilon_0 \widetilde{E_x^i} = \widetilde{J_x} \\ \dfrac{\partial \widetilde{H_y^i}}{\partial x} + i\omega\epsilon_0 \widetilde{E_z^i} = 0 \end{cases} \tag{B.5}$$

ruling the two states of polarization. From (B.4) comes

$$\Delta \widetilde{E_y^i} - \left(\omega^2 \epsilon_0 \mu_0\right) \widetilde{E_y^i} = 0. \tag{B.6}$$

The electron is coming from $z \to \infty$, there is no "original" source for $\widetilde{E_y^i}$. Thus, the only solution of Eq. (B.6) is zero: in the plane of incidence, the incident field is TM polarized.
The solution of (B.5) is

$$\widetilde{H_y^i} = -\frac{q}{2} \mathrm{sgn}(z - z_0) \exp\left(i\alpha_0 x + i\gamma_0 \left|z - z_0\right|\right) \tag{B.7}$$

where $\gamma_0 = i\sqrt{\alpha_0^2 - k_0^2}$, $k_0 = \frac{\omega}{c}$ and *sgn* names the sign function [12]. $\widetilde{E_x^i}$ and $\widetilde{E_z^i}$ can be directly calculated from $\widetilde{H_y^i}$. An important conclusion is that γ_0 is imaginary ($\alpha_0^2 > k_0^2$ follows from $v_0 < c$). Thus, the van den Berg model describes the incoming waves diffracted by the grating as a set of evanescent plane waves. We introduce $\lambda_e = 2\left|\gamma_0\right|$ (see 2.1 for discussion).

B.2 Diffracted field

A similar approach gives the equations satisfied by $\{\widetilde{\overrightarrow{E^r}}, \widetilde{\overrightarrow{H^r}}\}$

$$\begin{cases} \overrightarrow{\nabla} \times \widetilde{\overrightarrow{H^r}} + i\omega \widetilde{\overrightarrow{E^r}} = \overrightarrow{0} \\ \overrightarrow{\nabla} \times \widetilde{\overrightarrow{E^r}} - i\omega \widetilde{\overrightarrow{H^r}} = \overrightarrow{0} \end{cases} \tag{B.8}$$

$$\begin{cases} \overrightarrow{n} \times \left(\widetilde{\overrightarrow{E^i}} + \widetilde{\overrightarrow{H^r}}\right) = \overrightarrow{0} \text{ on } \Gamma \\ \overrightarrow{n} \cdot \left(\widetilde{\overrightarrow{H^i}} + \widetilde{\overrightarrow{H^r}}\right) = 0 \text{ on } \Gamma \\ \text{radiation condition} \end{cases} \tag{B.9}$$

where $\overrightarrow{n}$ is unitary and locally tangent to the grating surface denoted Γ. Eqs. (B.8) rule the propagation of the diffracted waves when Eqs. (B.9) represent the boundary conditions for a perfectly conducting surface denoted Γ. The *radiation condition* means that the propagating waves are bounded when $z \to \infty$. In the same way as the incident vectorial problem was restricted to two scalar problems (corresponding to the two independent states of polarization), we only study the performance of the y component of the Fourier transform of the fields. At this stage, no additional hypotheses are necessary to mathematically define the problem. But the periodicity of the grating in the x direction simplifies the diffracted field according to Curie's principle; one can write the Fourier series expansion

$$\widetilde{H_y^r}(x, z, \omega) = \sum_{-\infty}^{\infty} \widetilde{H_{y,n}^r}(z, \omega) \exp(i\alpha_n x) \tag{B.10}$$

where

$$\alpha_n = \alpha_0 + \frac{2\pi n}{d}. \tag{B.11}$$

The same work could be done with $\widetilde{E_y^r}(x,z,\omega)$, but we already know that $\widetilde{E_y^r}(x,z,\omega)=0$ thanks to 1.1.3. Inserting Eq. (B.10) in Eqs. (B.8) gives the *Rayleigh expansions* [17]

$$\widetilde{H_y^r}(x,z,\omega)=\sum_{-\infty}^{\infty}\widetilde{H_{y,n}^r}(\omega)\exp(i\alpha_n x+i\gamma_n z) \tag{B.12}$$

with $\gamma_n=\sqrt{k_0^2-\alpha_n^2}$. From a physical point of view, the waves propagate towards the positive z direction: $\Re(\gamma_n)>0$. Moreover, the radiation condition implies $\Im(\gamma_n)>0$. $\widetilde{H_{y,n}^r}(\omega)$ and $\widetilde{E_{y,n}^r}(\omega)$ are called *Rayleigh coefficients*.

B.3 Smith-Purcell propagation condition

Expanding the condition $\Re(\gamma_n)>0$ we find that the propagative orders must satisfy

$$X^2+\frac{2d}{\lambda\beta}X+\left(\frac{d}{\lambda\beta\gamma}\right)^2\leqslant 0 \tag{B.13}$$

Suppose there are two solutions $\{X_1,X_2\}$ with $X_1<X_2$. Then

$$n\in[\![\lceil X_1\rceil,\lfloor X_2\rfloor]\!] \tag{B.14}$$

The condition (B.13) isn't verified for X=0, and $X_{min}<0$, therefore $X_2<0$. From a physical point of view, λ in Eq. (2.2) is positive and cannot diverge, which also involves $n<0$. Using recent experiments at CLIO [20] as reference data, $\lambda\sim 1$ mm, $d\sim 8$ mm, $E\sim 50$ Mev ($E=\gamma mc^2$ involves $\gamma\sim 100$, $1-\beta\sim 5\times 10^{-5}$), orders of magnitude for n are: $-16\leqslant n\leqslant -1$. With Eq. (2.2) and $|\cos\theta|<1$, one can derive the bounds for the emitted wavelength in the *n-th* order:

$$\frac{1}{|n|}\left(\frac{1}{\beta}-1\right)\leqslant\lambda\leqslant\frac{1}{|n|}\left(\frac{1}{\beta}+1\right) \tag{B.15}$$

The higher $|n|$ is, the smaller the corresponding diffracted wavelength range is. A study of diffraction for *echelette* gratings also shows that the intensity of high orders is smaller. These two arguments justify why we only consider the first order $n=-1$ in this report.

B.4 Grating problem

The *grating problem* consists in finding the values of the Rayleigh coefficients introduced with Eqs. (B.7), (B.12). One can define a "modal" efficiency

$$|R_n|^2=\left|\frac{\widetilde{H_{y,n}^r}(\omega)}{\widetilde{H_y^i}(\omega)}\right|^2 \tag{B.16}$$

With the properties of the Fourier transform, this definition is consistent with classical diffraction efficiencies η_p of Eq. (1.2): $|R_n|^2\equiv\eta_p$. An important implication is that we can apply the grating property (preservation of polarization) to Smith-Purcell radiation. the incident field is TM polarized, therefore the Smith-Purcell radiation is also TM polarized (cf. 1.1.3). R_n is the ratio of the temporal mean value of incident and diffracted Pointing vectors. The interests of such R_n are: compatibility with grating definition of efficiencies, independence with charge value and energy.

B.5 Radiated energy

The energy per angle radiated in the θ direction for one electron can be written as [12, 21]

$$\left.\frac{\partial W_n}{\partial \theta}\right|_1 = \frac{q^2 n^2}{2\pi\epsilon_0 d} \frac{\sin^2\theta}{\left(\frac{1}{\beta} - \cos\theta\right)^3} \left| < \overrightarrow{\Pi_n'} \cdot \overrightarrow{u_n'} > \right| \tag{B.17}$$

Eq. (B.7) gives $< \overrightarrow{\Pi^i} \cdot \overrightarrow{u^i} > \equiv \frac{q^2}{4} \exp(-2\,|\gamma_0|\, z_0)$, then we find

$$\left.\frac{\partial W_n}{\partial \theta}\right|_1 = \frac{q^2 n^2}{8\pi\epsilon_0 d} \frac{\sin^2\theta}{\left(\frac{1}{\beta} - \cos\theta\right)^3} |R_n|^2 \exp(-\frac{z_0}{\lambda_e}) \tag{B.18}$$

where $\lambda_e = 2\,|\gamma_0|$ has the dimension of length. From $\gamma_0 = i\sqrt{\alpha_0^2 - k_0^2}$ it comes $|\gamma_0| = \dfrac{2\pi c}{v_0 \lambda \gamma}$ where γ is the Lorentz factor. Introducing Eq. (2.2) one can rewrite λ_e as

$$\lambda_e = \frac{2\pi n c}{v_0 \gamma d \left(\dfrac{1}{\beta} - \cos\theta\right)} \tag{B.19}$$

C

Asymmetric Gaussian parameters

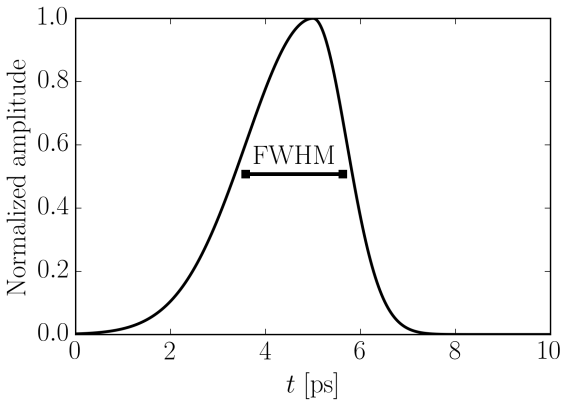

Figure C.1: Longitudinal profile T

We've chosen to model the longitudinal bunch profile as an asymmetric Gaussian. Note FWHM the full width at half maximum, and define a standard deviation $\sigma = \frac{\text{FWHM}}{\sqrt{2\log 2(1+\epsilon)}}$, where ϵ is an asymmetric factor. If t_c is the time for which the electron distribution is maximum (on Fig. C.1, $t_c \approx 5$ ps), then the longitudinal profile is:

$$T(t) = \begin{cases} \exp(-\dfrac{(t-t_c)^2}{2\sigma}, & \text{if } t < t_c \\ \exp(-\dfrac{(t-t_c)^2}{2\epsilon\sigma}, & \text{if } t > t_c \end{cases} \tag{C.1}$$

Bibliography

[1] S.J. Smith, E.M. Purcell, "Visible Light from Localize d Surface Charges Moving across a Grating", *Phys. Rev.* **92**, 4 (1953)

[2] D. Jackson, *Classical Electrodynamics*, Wiley (1963).

[3] E. Bründermann, H.-Z. Hübers, M.F. Kimmitt *Terahertz Techniques*, Springer (2012).

[4] E.G. Loewen, E. Popov, *Diffraction Gratings and Applications*, Dekker (1997).

[5] R. Petit, *Electromagnetic Theory of Gratings*, Springer (1980).

[6] E.G. Loewen, M. Nevière, D. Maystre, "Grating efficiency theory a it applies to blazed and holographic gratings", *Appl. Opt.* **16**, 10 (1977)

[7] D. Maystre, *Plasmonics*, "Theory of Wood's Anomalies ", Springer (2012).

[8] D. Maystre, *Gratings: Theory and Numeric Applications*, "Analytic Properties of Diffraction Gratings ", PUP (2012).

[9] H. Rathgen, *Superhydrophobic Surfaces: from Fluid Mechanics to Optics*, Ph.D thesis Twent University (2008)

[10] M.G. Moharam "Formulation for stable and efficient implementation of the rigorous coupled-wave analysis of binary gratings ", *Am. Opt. Soc.* **12**, 5 (1995)

[11] J.J Hench, Z. Strakos, "The RCWA method", *Elec. Tr. Num. An.* **31**, 331-337 (2008)

[12] O. Haeberlé, *Electromagnetic Radiation Generated by Relativistic Electrons interacting with a Diffraction Grating*, Ph.D thesis Université de Haute-Alsace (1994)

[13] G. Toraldo Di Francia, "On the theory of some Cerenkovian effects", *Nuovo Cimento* **16**, 61 (1960)

[14] J.H. Brownell, J. Walsh, G. Doucas, "Spontaneous Smith-Purcell radiation described through induced surface currents", *Phys. Rev. E* **57**, 1 (1998)

[15] J.H. Brownell, G. Doucas, "Role of the grating profile in Smith-Purcell radiation at high energies", *Phys. Rev.* **8**, 091301 (2005)

[16] H.L. Andrews, G. Doucas, N. Delerue, "Longitudinal profile monitors using Coherent Smith-Purcell radiation", *Phys. Res. A* **740**, 212-215 (2014)

[17] P.M. van den Berg, "Smith-Purcell radiation from a line charge moving parallel to a reflection grating", *J. Opt. Soc. Am.* **63**, 6 (2005)

[18] O. Haeberlé, "Reciprocity theorem for Smith-Purcell radiation", *Opt. Comm.* **141**, 237-242 (1997)

[19] P.B. Johnson, R.W. Christy "Optical Constants of the Noble Metals", *Phy. Rev. B* **6**, 12 (1972)

[20] N. Delerue, S. Jenzer, V. Khodnevych, "Study of Short Bunches at the Free Electron Laser Clio", *IPAC*, MOPMB005 (2016)

[21] A.P. Potylitsyn, D.V. Kartovets, "Comparison of Smith-Purcell radiation models and criteria for their verification", *Phys. Rev.* **9**, 080701 (2006)

[22] K. Murata, H. Tanaka "Surface-wetting effects on the liquid?liquid transition of a single-component molecular liquid", *Nature Com.* **1**, 16 (2010)

[23] Thorlabs, 6th July 2016, http://www.thorlabs.com/images/tabImages/750_1200_Ruled_Grating_Efficiency_Graph_780.jpg

[24] D. Delbeke, *Design and Fabrication of a Highly Efficient Light-Emitting Diode: the Grating-Assisted Resonant-Cavity Light-Emitting Diode*, Ph.D thesis University Gent (2002)

[25] Photonics group, Departement of Information Technology, Ghent University, 12th July 2016, http://photonics.intec.ugent.be/